Universiteit
Leiden
The Netherlands

Laboratory studies of water ice in space : optical and photochemical properties

Kofman, V.

Citation
Kofman, V. (2019, June 19). *Laboratory studies of water ice in space : optical and photochemical properties*. Retrieved from https://hdl.handle.net/1887/74048

Version:	Not Applicable (or Unknown)
License:	Leiden University Non-exclusive license
Downloaded from:	https://hdl.handle.net/1887/74048

Note: To cite this publication please use the final published version (if applicable).

Cover Page

Universiteit Leiden

The handle http://hdl.handle.net/1887/74048 holds various files of this Leiden University dissertation.

Author: Kofman, V.
Title: Laboratory studies of water ice in space : optical and photochemical properties
Issue Date: 2019-06-19

Chapter 5

The photochemistry of glycine in water ice

Abstract
We have investigated the protective and photochemical role of amorphous solid water (ASW) upon vacuum ultraviolet (VUV) irradiation of embedded glycine (Gly, NH_2CH_2COOH) using *in situ* and simultaneous UV-vis and IR spectroscopy. The photodegradation of Gly is monitored by its dissociation products. Gly photolysis in a water-free matrix results in CO_2 and $\cdot$CN/HCN. In ASW, CO_2 and HCN/OCN^- are formed, indicating that water participates in the VUV induced photoprocesses. Quantitative results are derived based on the photodestruction rates as a function of H_2O thickness. These indicate that approximately 152 nm of compact water ice is needed to decreases the VUV flux by half. We use this result to calculate the survival chance of Gly under the VUV radiation present in dark molecular clouds.

5.1 Introduction

For many years, comets have been considered as a potential source of prebiotic molecules to planets like the early Earth (Chyba and Sagan, 1992). This hypothesis is supported by the recent detection of glycine (Gly) and other organic molecules on comet 67P/Churyumov-Gerasimenko (Goesmann et al., 2015; Altwegg et al., 2016) and by studies of organic matter in cometary dust grains collected from the tail of 81P/Wild by the Stardust mission (Sandford et al.,

Kofman, V., Jense H. T., Ligterink N. F. W., ten Kate, I. L. and Linnartz, H. "The role of water ice on the vacuum UV photodegradation of embedded glycine" *In prep.*

2006). Other potential extraterrestrial sources of organic matter are meteorites, asteroids and interplanetary dust particles (Chyba and Sagan, 1992; Ehrenfreund et al., 2002; Frantseva et al., 2018), all of which can contain significant amounts of organic carbon, including amino acids (Cody and Alexander, 2005; Schmitt-Kopplin et al., 2010; Elsila et al., 2016).

In recent years, specialized laboratory studies have shown that large organic molecules can form from rather simple precursor species in and on the icy layers that cover nano- to micrometer-sized interstellar dust grains (Gibb et al., 2004; Boogert et al., 2015). Examples of reactions resulting in these complex organic molecules (COMs) are the hydrogenation of CO to form formaldehyde, methanol and larger saturated carbohydrates, such as glycoaldehyde, ethylene glycol and glycerol (Hiraoka et al., 1994; Zhitnikov and Dmitriev, 2002; Fuchs et al., 2009; Chuang et al., 2016; Fedoseev et al., 2017); the UV irradiation of methanol ice (Öberg et al., 2009a; Henderson and Gudipati, 2015; Paardekooper et al., 2016) or methane ice (Baratta et al., 2002; Cottin et al., 2003; Bossa et al., 2015a) which were all shown to result in the formation of small sugars, sugar alcohols and ethers as well as ethane and other alkanes. These studies are in line with work in which *ex situ* analysis of residues, remaining after prolonged VUV irradiation of ice mixtures consisting of H_2O, CO, CO_2, CH_3OH, NH_3, and HCN, were shown to contain a surprising variety of large organic molecules (Muñoz-Caro et al., 2002; Bernstein et al., 2002; Nuevo et al., 2010; Meinert et al., 2016; Danger et al., 2016). Thermal processing of astronomical ices (i.e. from 10 to 300 K) is also thought to be involved in the formation of more complex molecules (Noble et al., 2013; Theulé et al., 2013). In many of these reactions, the solid phase acts as a molecular reservoir and a third (catalytic) body facilitating surface reactions and capable to absorb the excess formation energy released in radical recombination reactions (Hama and Watanabe, 2013; Linnartz et al., 2015; Butscher et al., 2017).

In all these processes, the formation and destruction of molecules are closely related. In order for the organic material found on icy dust grains to survive on comets or interplanetary dust particles, it needs to withstand a significant dose of vacuum UV (VUV) radiation, either from stellar radiation or due to emission from cosmic ray excited molecular hydrogen. The goal of the work presented here is to investigate how well COMs formed in ice environments are protected by that same environment, using Gly as a representative for other COMs.

The planetary science community has been focusing in the past on the photostability of amino acids, and mostly in their pure form. Amino acids

are present in all life as we know it, and are thus highly relevant from an astrobiological perspective. Amino acids contain an amine group ($-NH_2$) and a carboxylic acid group ($-COOH$), both important and ubiquitous in biological molecules as they can react to form the peptide bonds, the basis of proteins. These groups, and thus amino acids, are relatively reactive. Studies over the last years have focused on the survival of Gly, the smallest amino acid, exposed to UV-light (Ehrenfreund et al., 2001; ten Kate et al., 2005; Orzechowska et al., 2007; Johnson et al., 2012), protons (Gerakines et al., 2012), X-rays (Pernet et al., 2013; Portugal et al., 2014) and electrons (Maté et al., 2015). These studies have shown that glycine is easily destroyed by the different types of external processing, resulting in the formation of CO_2 and HCN (Sagstuen et al., 2004). The production of HCN from Gly was suggested to involve methylamine (CH_3-NH_2) and methylimine ($CH_2=NH$) as intermediate species, but so far no evidence for these species has been found (Ehrenfreund et al., 2001). Many of the aforementioned studies use pure Gly or Gly in water at relatively high concentrations, raising the question to what extent Gly may react with itself or produced fragments; high mixing ratios of Gly in water may affect the outcome of the photochemical reactions.

In this chapter, we investigate the photodestruction of Gly embedded in amorphous solid water (ASW), over a range of (lower) concentrations, with a particular focus on the formation rates of the reaction products. The formation rates are used to determine to what extent water ice can act as a radiative shield, absorbing VUV light, and protecting embedded molecules. In fact, as water is the most abundant ice in space, this would provide an effective way to preserve COMs.

From the absorption cross section of water ice in the VUV, it is in principle possible to derive the amount of light absorbed by a layer of water, and estimate how likely molecules are to survive VUV radiation when inside water ice. The absorption spectrum of water in the VUV has been recorded between 120 and 165 nm (Mason et al., 2006; Cruz-Diaz et al., 2014). Using the available literature values (which considered the average absorption cross section) this results in a 50 % VUV flux decrease between 120-165 nm for every 62 nm of compact ASW. Using the average cross section likely overestimates the shielding however, as the VUV absorbance of water decreases strongly above 160 nm, thus allowing the photons to penetrate deeper into the ice. Nor does not include the role of chemical processes taking place. Absorption of a VUV photon by water ice is known to produce $\cdot$H and $\cdot$OH, as well as O_2 and H_2O_2 as secondary products (Gerakines et al., 1996; Öberg et al., 2010; Yabushita et al., 2013). As

radical species are known to be more mobile at higher temperatures, this is an important aspect of understanding the reactivity of the water matrix on the embedded species. Moreover, the VUV absorption decreases above 160 nm, where the molecular H_2 Lyman band system still causes prominent emission, both in dark clouds and the hydrogen plasma lamps used in the laboratory. Photons with energies in this range are still capable of photodissociating COMs. For these reasons, here also an experimental study is performed. Our study provides a different method for determining the penetration depth of VUV photons in ASW, taking into account photochemistry, including those with wavelengths longer than 160 nm.

By first constraining the photochemistry of Gly in a chemically inert argon matrix, and then comparing these results with those of similar experiments performed in ASW, this allows assessing the effect of water ice on the photostability of Gly. As the experiments are studied both using UV-vis and IR spectroscopy, both electronic transitions of transients species, as well as the vibrational spectra of the stable end products are measured. The experiments are carried out with ices of increasing thickness between 150 and 700 nm, with correspondingly decreasing concentrations, and at two different temperatures (10 and 100 K). The results for the different temperatures and ASW thicknesses are compared. Based on these results we calculate how much ASW is needed for Gly to survive as a function of VUV flux.

5.2 Experimental details

Gly is co-deposited with argon or water at temperatures as low as 10 K. The ice mixtures are then irradiated with VUV radiation for three hours. Gly destruction and formation of products is monitored *in situ* and simultaneously with UV-vis and Fourier transform infrared (FTIR) spectroscopy. A detailed description of the experimental setup and sample preparation follows below.

5.2.1 Experimental setup

The new experimental setup used for this study has been described in detail in Chapter 2. It consists of a cryostat mounted in a high vacuum chamber with a base pressure of $5{\cdot}10^{-8}$ mbar. At the tip of the cryostat, a UV to IR transparent BaF_2 (0.15 - 16.7 μm) window is mounted that is used as a substrate onto which ices are grown, typically using direct deposition that results in compact ices.

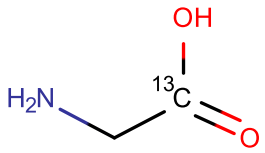

FIGURE 5.1: Molecular structure of the used ^{13}C labeled glycine (Gly). The ^{13}C isotopic substitution is on the carbonyl carbon.

A custom built temperature controlled oven is used to sublimate non-volatile species that are subsequently deposited onto the substrate. In Chapter 2 we demonstrated the sublimation rate from our oven reproduces very well on a day to day basis, allowing accurate reproduction of the column densities of Gly (see Chapter 2, Fig. 2.5). Gly is simultaneously deposited with Ar or H_2O, dosed through a separate deposition line. This allows the preparation of mixtures at any ratio as the amount of Ar/H_2O is varied independently from Gly.

The resulting ices are studied in two wavelength ranges, using UV-vis light from a Xe-arc lamp (200-760 nm), and a Fourier transform infrared spectrometer (FTIR, 2.5 - 16.7 μm). Both systems can be used simultaneously, allowing us to link electronic and vibrational spectral features, see Kofman et al. (2018). The prepared ices are irradiated using a microwave discharge hydrogen lamp peaking around the Ly-α wavelength (121 nm) and emitting a broad (molecular H_2) band around 160 nm (Warneck, 1962; Cruz-Diaz et al., 2014; Ligterink et al., 2015). These lamps have a spectral output similar to the interstellar radiation field in the VUV (Heays et al., 2017). A MgF_2 window allows transmission of all wavelengths longer than 116 nm to the ice. The absolute flux of our VUV lamp has been determined by oxygen-ozone actinometry (Cottin et al., 2003; Fulvio et al., 2014) and is $1.7\pm0.3\cdot10^{15}$ photons cm^{-2} s^{-1}.

5.2.2 Sample preparation and processing

Commercially available 1-^{13}C-Gly (99 %) is used without further purification. Isotopically labeled Gly is used to discriminate between $^{13}CO_2$ formed upon dissociation and CO_2 due to potential background gas contamination. The molecular structure and the location of the isotopically enriched carbon atom are shown in Fig. 5.1. Liquid nitrogen dried argon (5.0 purity), and demineralized water, degassed by a series of freeze-pump-thaw cycles prior to use,

are taken as precursor materials for the matrix environment. The thickness of the matrix layer is regulated by the setting of a precision dosing valve. Different thicknesses of water ice are realized by setting higher flow rates, and as the deposition time is kept the same this results in increasingly lower concentrations of Gly in the ice. For each experiment, the oven is pre-heated to 105 °C, before rotating the sample to face the oven and co-depositing argon or water with the Gly to produce a homogeneous mixture. In each of the experiments, the column density of Gly is in the order of $8{\cdot}10^{15}$ molecules cm^{-2}. The Ar experiments are performed at 10 K, and the two investigated ASW temperatures are 10 and 100 K. The ice thickness is determined from the infrared integrated column densities of H_2O, as no assumptions regarding the ice densities have to be made using this method. Water column densities used are between $4{\cdot}10^{17}$ and $2{\cdot}10^{18}$ molecules cm^{-2}, corresponding to roughly 150-700 nm for fully compact ice (see 5.2. The ice mixtures are then irradiated for 3 hours using the microwave discharge hydrogen lamp corresponding with a total fluence in the order of $1.8{\cdot}10^{19}$ photons cm^{-2}. During the VUV irradiation, UV-vis and infrared spectra are recorded continuously.

It should be noted that the sublimation of Gly produces the neutral form, even though in its crystalline form at room temperature the molecule is known to occur in its zwitterionic form $NH_3^+CH_2{-}COO^-$. The zwitterionic form is preserved when embedded in the ice until it is heated above ∼100 K (Maté et al., 2011; Gerakines et al., 2012). The latter study showed that only at temperatures of 140 K Gly is fully converted to its zwitterionic form. For our study this implies that Gly will be predominantly in its neutral form; this is important as its electronic absorption spectrum in the zwitterionic form is likely different from the one in the neutral form.

5.3 Results and Discussion

5.3.1 Photochemistry of glycine

Gly has no detectable transitions in the UV-vis range, and only in argon can we observe its infrared absorption features. At the Gly:ASW concentrations used here, the Gly infrared signals are obscured by the much stronger water features. Hence, we focus on the formation of photoproducts to characterize the Gly stability on VUV irradiation, i.e. we take explicitly take into account the photochemistry. The main photoproducts detected are $^{13}CO_2$, HCN, $\cdot$CN,

TABLE 5.1: Molecular parameters of the four VUV induced Gly fragments. Absorption maxima are in water ice.

Species	Detection	Absorption max. in H_2O	Transition strength	Reference
$^{13}CO_2$	FTIR	2279 cm^{-1}	$7.8{\cdot}10^{-17}$ cm $molecule^{-1}$	Gerakines et al. (1995)
HCN	FTIR	2090 cm^{-1}	$5.1{\cdot}10^{-18}$ cm $molecule^{-1}$	Bernstein et al. (1997)
$\cdot$CN	UV-vis	388 nm	$f = 0.0032$	Danylewych and Nicholls (1978)
OCN^-	FTIR	2170 cm^{-1}	$1.6{\cdot}10^{-18}$ cm $molecule^{-1}$	van Broekhuizen et al. (2005)

and OCN^-. Their respective absorption maxima and transition strengths are listed in Table 5.1. Note that the absorption of the radical species $\cdot$CN is in the UV-vis, whereas the other fragments absorb in the IR. We use these band strengths to derive column densities and formation rates.

Fig. 5.2 shows a zoom-in of the spectral region in the infrared where $^{13}CO_2$, OCN^-, and HCN have vibrational transitions. The integrated area of the peaks, which is used in the next section, are indicated in gray. For each experiment (i.e. argon 10 K, water 10 K and water 100 K) three spectra are shown which correspond to, i) before VUV irradiation, ii) after 1200 seconds and iii) after 3600 seconds of photoprocessing. The spectra are offset for clarity. The spectra in Fig. 5.2 show that in each of the experiments significant amounts of $^{13}CO_2$ is formed upon VUV irradiation. Both HCN and OCN^- are formed as well in all of the experiments, but at very different abundances.

In Fig. 5.3 we show the measured abundance of the species listed in Table 5.1 and Fig. 5.2 as a function of time, i.e. increasing fluence. The results of three different experiments are shown: Gly:Ar at 10 K, Gly:H_2O at 10 K and Gly:H_2O at 100 K. Time t=0 is defined as the start of the VUV irradiation. All panels show the column densities in molecules per square centimeter, which are calculated using the integrated absorbance of the respective transitions. $^{13}CO_2$ is shown in Fig. 5.3a, HCN in Fig. 5.3b, $\cdot$CN in Fig. 5.3c and OCN^- in Fig. 5.3d.

Comparing the $^{13}CO_2$ production in Ar and H_2O in Fig. 5.3a, we see that the signal increases at the same rate for the first few hundred seconds in Ar and ASW at 10 K. This is in agreement with previous studies by Ehrenfreund et al., 2001, who reported similar half-life times of Gly in Ar and Gly in H_2O; and demonstrated that for thin ices the water environment does not enhance the VUV photostability of Gly. For thicker water layers we will see that this is not the case anymore, as will be discussed in section 5.3.2. The $^{13}CO_2$ abundance in Ar starts to decrease after roughly 20 minutes, indicating that $^{13}CO_2$ is destroyed at a larger rate than it is formed, whereas the net $^{13}CO_2$ production

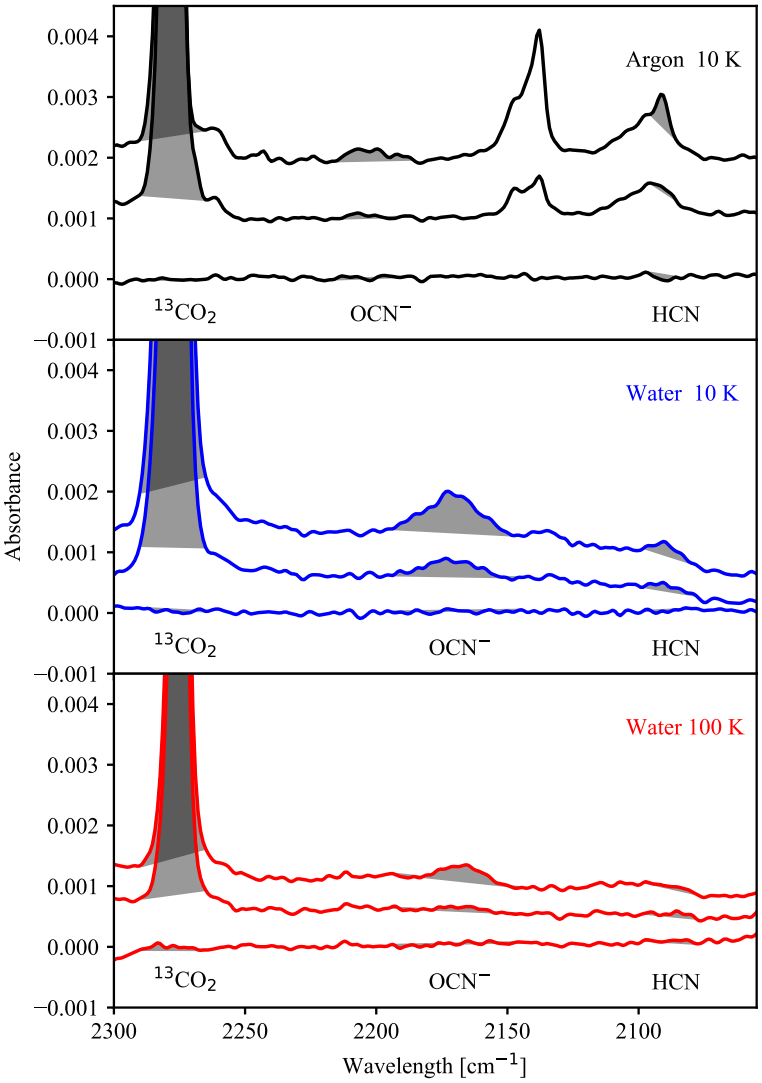

FIGURE 5.2: Infrared spectra of the three different experiments discussed in section 5.3.1. The top panel shows the Gly in argon at 10 K, the middle panel in water at 10 K, and the bottom panel in water at 100 K. Each of the plots shows three spectra, one before irradiation, one after roughly 1200 seconds and one after 3600 seconds of irradiation. The locations of the absorption of $^{13}CO_2$, OCN^- and HCN are indicated, as well as the areas under the features. Spectra are offset for clarity. Note that the absorbance of OCN^- is shifted, and a broad feature is present under the HCN absorption in the argon matrix.

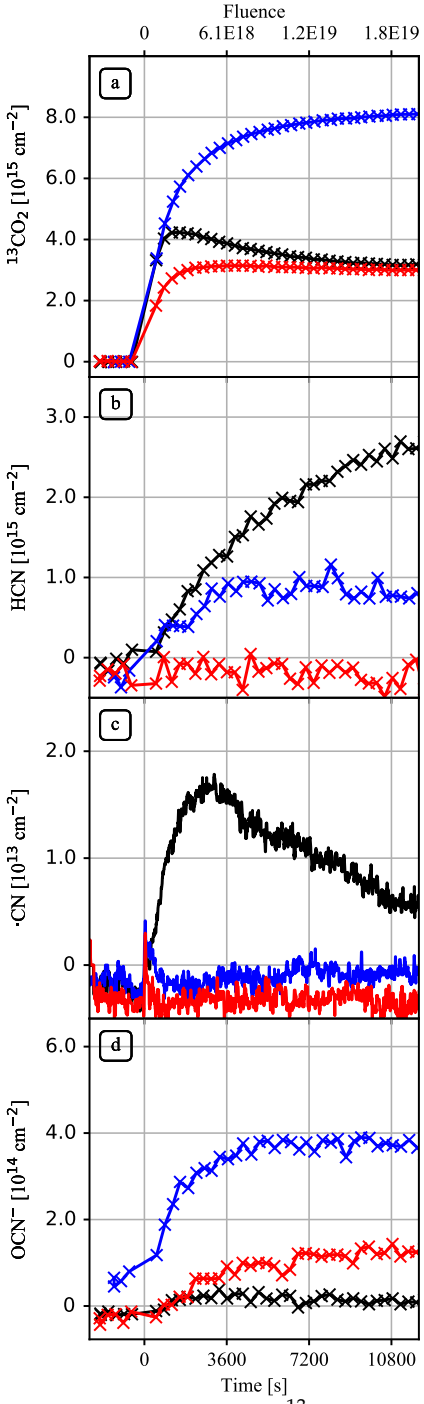

FIGURE 5.3: Column densities of (a) $^{13}CO_2$, (b) HCN, (c) ·CN and (d) OCN^- in three different experiments as a function of time, i.e. of fluence. The black lines are Gly:Ar at 10 K, blue lines Gly:H_2O at 10 K and red is Gly:H_2O at 100 K. The species are indicated in the label on the vertical axis, note that the different panels have different scales. The samples are irradiated from t = 0 to 10800 seconds.

continues in the water matrix. In ASW at 100 K, the $^{13}CO_2$ production is much less efficient. The reaction progresses slower, and the total column density stabilizes after roughly 2000 seconds. It should be noted that CO_2 is not expected to escape from the ice matrix even at 100 K. We confirmed this by monitoring the CO_2 column densities after irradiation and prior to heating of the sample.

The formation of HCN, shown in Fig. 5.3b, is much slower than the formation of $^{13}CO_2$. This suggests that HCN forms as an indirect photoproduct from Gly. The production of HCN is more efficient in Ar than in ASW, which is in line with the observation that it is a secondary product, as more side reactions can be expected to occur in ASW. The fact that almost no HCN is detected in the 100 K experiment corroborates this theory, as the mobility of radical species is expected to be enhanced at higher temperatures.

The formation of $\cdot$CN, absorbing around 380 nm (in the UV-vis), is shown in Fig. 5.3c. We see that $\cdot$CN is produced at the highest rate at the start of the irradiation, suggesting it may be the reactive intermediate through which HCN forms. We do not find significant $\cdot$CN signals in the UV-vis spectra in the Gly:H_2O experiments, which shows that $\cdot$CN is likely directly consumed in reactions that involve water or water photoproducts. Considering that $\cdot$CN may be the source of the formed HCN, the absence of $\cdot$CN in the water experiments may explain the low abundance of HCN in the ASW experiments.

Fig. 5.3d shows the production of OCN^-, a well known interstellar ice constituent (van Broekhuizen et al., 2005), but not *a priori* expected here following the reactions reported in the literature (Ehrenfreund et al., 2001; Sagstuen et al., 2004). Comparing OCN^- abundances at 10 and 100 K in the Gly:H_2O experiments, we see much less OCN^- forming at the higher temperature. A reaction between $\cdot$OH radicals and $\cdot$CN would explain the abundance of OCN^- and the absence of $\cdot$CN in the ASW experiments. Note also that OCN^- is a known photoproduct from the irradiation of HCN in water (Gerakines et al., 2004).

Combining the information gained from the UV-vis and FTIR experiments in Ar, we find that the photolysis of Gly results in the formation of $\cdot$CN and $^{13}CO_2$. Hydrogenation by H atoms formed in this process yields the formation of HCN. This reaction scheme explains the absence of evidence of methylamine and methylimine in previous experiments. If Gly is placed in an ASW matrix, this adds further chemical complexity to the reaction chain, resulting in the formation of OCN^- and changes in the HCN, $\cdot$CN and CO_2 production rates.

5.3.2 Photodegradation rates of Gly as a function of H_2O thickness

Monitoring the fluence dependency of the abundances of the photoproducts provides a quantitative tool to characterize the photostability of Gly, even when the destruction of Gly itself cannot be directly traced. To constrain the shielding effect of ASW, we perform a series of experiments where the ASW thickness is increased, and quantify the destruction rate of Gly at each ice thickness. Ten experiments were performed, five in ASW at 10 K and five at 100 K; see Table 5.2 for the full list. We use the formation of $^{13}CO_2$ to monitor the progress of the photodestruction of Gly. With thicker ices, a larger fraction of the Gly will be embedded deeper in the ice where the effective VUV flux is lower. We use the resulting destruction rates, determined as a function of thickness, to calculate the VUV shielding of water.

In Fig. 5.4 we show the time-dependent column density of $^{13}CO_2$ for the total of 11 experiments we performed. Each experiment has a different ice thickness and is represented by a unique marker (see Table 5.2). The left panel of Fig. 5.4 shows five experiments performed in ASW at 10 K in blue, and one in Ar at 10 K in black. The five 100 K ASW experiments are shown in the right panel of Fig. 5.4 in red. The corresponding column density of $^{13}CO_2$ upon VUV irradiation is fit using:

$$[^{13}CO_2] = N_f(1 - \exp(-k_{pr}t)), \tag{5.1}$$

N_f is the total amount of produced $^{13}CO_2$ in [molecules cm^{-2}], t is the time, and k_{pr} is the production rate constant. Considering that the starting column densities of Gly are approximately the same, the initial $^{13}CO_2$ production rate and the value N_f constrain the effect of the thickness of water on the photostability of Gly. The $^{13}CO_2$ formation rate, R_d, is given by:

$$R_d = k_{pr}N_f \tag{5.2}$$

To determine k_{pr} and N_f, we take into account only the first 1500 seconds of irradiation (corresponding to a fluence of $2.6\pm0.5\cdot10^{18}$ photons cm^{-2}), as the column density of $^{13}CO_2$ appears to stabilize after this in several experiments, especially in the experiments performed at 100 K. The absence of additional $^{13}CO_2$ production suggests that either the reaction has fully progressed, or that $^{13}CO_2$ is being consumed, as is clearly seen in the Gly:Ar experiments (Fig. 5.3a). The kinetics of the $^{13}CO_2$ formation are consistent with the latter:

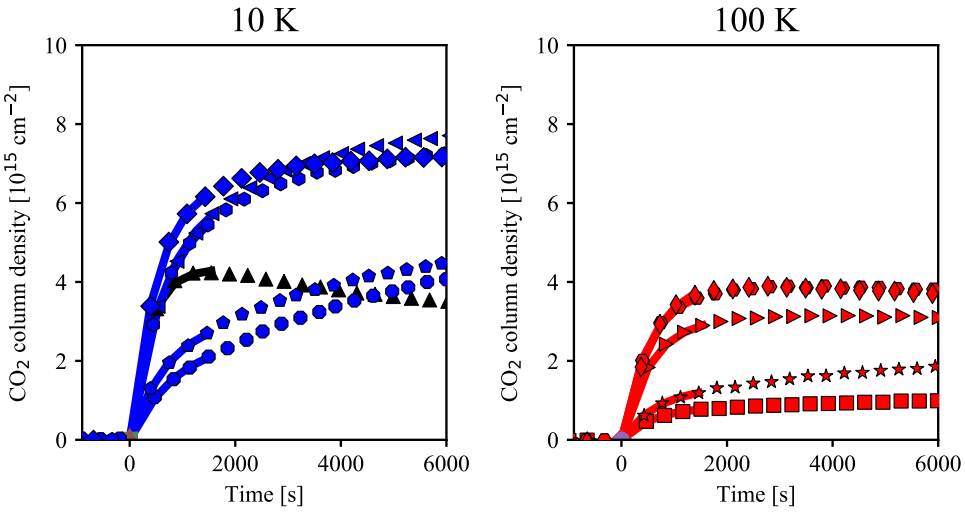

FIGURE 5.4: Column densities of $^{13}CO_2$ produced in: (a) Gly:H_2O at 10 K (blue) and Gly:Ar at 10 K (black) and (b): Gly:H_2O at 100 K (red). The thick solid line is the fit of Eq. 5.1. The experiments are plotted as a function of time. VUV irradiation is started at $t = 0$. Each experiment has a unique marker, see Table 5.2.

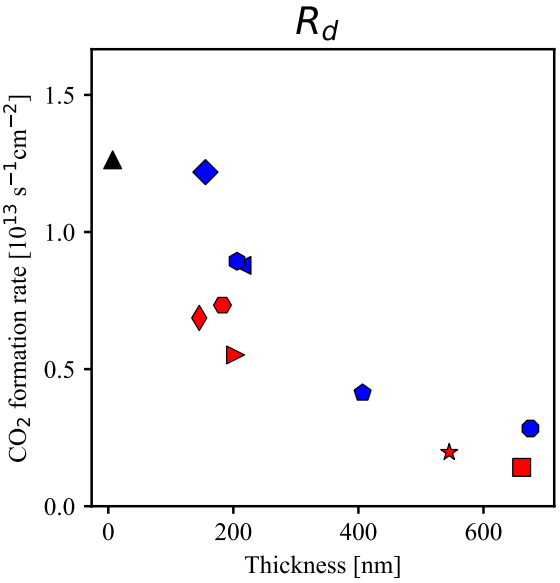

FIGURE 5.5: The $^{13}CO_2$ formation rates, R_d, of the different experiments shown as a function of the ice thickness. Each experiment has the same unique markers as Fig. 5.4 , also see Table 5.2.

photochemical reactions are expected to follow an exponential behavior for the production of reactants and this is clearly not the case for the $^{13}CO_2$ production at 100 K for irradiation times beyond 1500 s.

The fit parameters N_f and k_{pr} are listed for the different experiments in Table 5.2. We see that N_f and k_{pr} both decrease as a function of ASW thickness. The experiments performed at 100 K consistently show lower values of N_f and k_{pr}. All of the corresponding values of R_d are shown in Fig. 5.5 as a function of thickness. The blue markers are from the experiments at 10 K, and the red ones correspond to the experiments performed at 100 K.

Half-life times of Gly in ASW

The half-life times of Gly in the ASW experiments cannot directly be determined as no Gly signals can be recorded but instead, the photoproduct $^{13}CO_2$ is monitored. $^{13}CO_2$ formation can be linked quantitatively to Gly photofragmentation, but only when further reactions with $^{13}CO_2$ can be ruled out. In the experiments at 10 K, no $^{13}CO_2$ destruction is observed and we assume that the CO_2 production rate is equal to the Gly destruction rate ($k_{pr} = k_{de}$). We determine the half-life time of Gly in the cases where the photodestruction of Gly has fully progressed. This is true for the 10 K experiment with the lowest water column density. Using:

$$t_{\frac{1}{2}} = \frac{\ln 2}{k_{de}}, \tag{5.3}$$

with $k_{de} = 1.8 \cdot 10^{-3}$ s^{-1}, we calculate a half-life time of 380±20 seconds for the experiment at 10 K with an ice thickness of 155 nm (see table 5.2).

Ehrenfreund et al. (2001) reported a half-life time of Gly in water of 1000 seconds. This was for a water thickness of 0.2 μm and is approximately double our half-life time at this ice thickness (the 10 K experiment with a thickness of 206 nm). The amount of Gly used in that study is roughly ten times what is used in our study however, which may result in self-shielding, causing an increase in the half-life time.

TABLE 5.2: Overview of the Gly:H_2O and Gly:Ar experiments, and the resulting N_f, k_{pr} and R_d values.

Thickness [nm]	Temp. [K]	Mixing ratio Gly:matrix	N_f [molecules]	k_{pr} [s^{-1}]	R_d [molecules s^{-1} cm^{-2}]	Marker in Fig. 5.5
Ar	10	1:116	$4.3{\cdot}10^{15}$	$2.9{\pm}0.2{\cdot}10^{-3}$	$1.3{\cdot}10^{13}$	▲
155	10	1:61	$6.7{\cdot}10^{15}$	$1.8{\pm}0.1{\cdot}10^{-3}$	$1.2{\cdot}10^{13}$	◆
206	10	1:81	$6.2{\cdot}10^{15}$	$1.4{\pm}0.1{\cdot}10^{-3}$	$8.9{\cdot}10^{12}$	⬢
214	10	1:84	$6.5{\cdot}10^{15}$	$1.4{\pm}0.1{\cdot}10^{-3}$	$8.8{\cdot}10^{12}$	◀
407	10	1:160	$3.1{\cdot}10^{15}$	$1.3{\pm}0.1{\cdot}10^{-3}$	$4.1{\cdot}10^{12}$	⬟
675	10	1:265	$2.6{\cdot}10^{15}$	$1.1{\pm}0.1{\cdot}10^{-3}$	$2.8{\cdot}10^{12}$	⬢
145	100	1:57	$4.1{\cdot}10^{15}$	$1.7{\pm}0.1{\cdot}10^{-3}$	$6.9{\cdot}10^{12}$	♦
183	100	1:72	$3.9{\cdot}10^{15}$	$1.9{\pm}0.1{\cdot}10^{-3}$	$7.3{\cdot}10^{12}$	⬣
204	100	1:80	$3.1{\cdot}10^{15}$	$1.8{\pm}0.1{\cdot}10^{-3}$	$5.5{\cdot}10^{12}$	▶
545	100	1:214	$1.3{\cdot}10^{15}$	$1.5{\pm}0.1{\cdot}10^{-3}$	$2.0{\cdot}10^{12}$	★
661	100	1:260	$8.4{\cdot}10^{14}$	$1.7{\pm}0.1{\cdot}10^{-3}$	$1.4{\cdot}10^{12}$	■

5.3.3 Protection of the water matrix

We will now use the formation rates of $^{13}CO_2$, R_d at the different thicknesses, to quantify the shielding effect of water on the embedded Gly. The VUV flux inside the ice decreases with thickness as H_2O absorbs a part of the VUV photons. Thus, we expect the photodegradation rates of Gly to decrease in thicker ice layers. This is indeed what we conclude from Fig. 5.5 where a decreasing $^{13}CO_2$ formation rate for thicker ices is shown. The VUV flux in the ice decreases exponentially with depth inside the ice according to the Lambert-Beer law:

$$I_d = I_0 \exp\left(\frac{-d}{\delta}\right), \tag{5.4}$$

where I_d is the flux at depth d in the ice and δ is the attenuation constant, which translates to the amount of water required to decrease the flux by an amount $1/e$. I_0 is the unattenuated flux. The average flux inside the ice is obtained by integrating over d:

$$I_{av} = \frac{I_0\delta}{d}\left(1 - \exp\left(\frac{-d}{\delta}\right)\right). \tag{5.5}$$

The rate of a photochemical typically scales linearly with the incident flux, which is what we assume for our case. It follows:

$$R_d = \alpha \frac{I_0 \delta}{d}(1 - \exp(\frac{-d}{\delta})), \tag{5.6}$$

where α is the efficiency of the photochemical reaction (i.e. the product of the cross section and quantum yield). α will be eliminated by looking at the normalized formation rates. As d increases, $\exp(\frac{-d}{\delta})$ approaches zero, and the respective rates effectively scale as $\frac{\delta}{d}$: as the thickness d increases, the effectively exposed fraction of Gly decreases. We can now quantify the shielding effect of water, treating both sets of R_d at the 10 and 100 K separately. We normalize each series to the highest rate, which is the rate in the thinnest ice at that temperature, and fit $\frac{\delta}{d}$ to the normalized destruction rates. The result is shown in Fig. 5.6. The values for δ are very similar at both temperatures (151 at 10 K vs. 153 at 100 K) indicating that the light penetration is the same within our margins of error. Note however that the formal error quoted here does not include the uncertainty in the infrared band strength of water that is used to determine the ASW thickness (typically the error is assumed to be in the order of 20 %).

We can compare our δ-value with that as derived from Cruz-Diaz et al. (2014) who studied the VUV spectrum of ASW and reported 95 % and 99 % absorbing column densities. From their reported average cross section between 120 and 165 nm, we derive a value of δ = 61 nm, which is about a factor 2.5 smaller than derived from our work. The difference between these values likely comes from to the emission of the lamp above 160 nm, where water ice absorbs significantly less VUV light than the average of the spectrum, from which the shielding was calculated (Cruz-Diaz et al., 2014). In fact, our value for δ is more consistent with findings from studies where polycyclic aromatic hydrocarbons are irradiated with VUV light in water, where often several micrometers of water ice is used and find significant photodestruction and/or ionization (Bouwman et al., 2009).

5.3.4 Astronomical impact

We will now derive an equation that allows us to calculate the required ice thickness d_s for Gly to survive under a photon flux I_s for a given time t_s, depending on δ. As the half-life times directly scale with the flux, and the flux

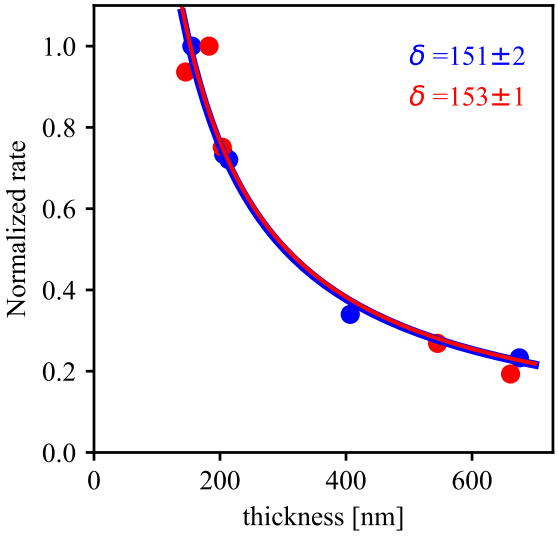

FIGURE 5.6: Normalized $^{13}CO_2$ formation rates in the different Gly:H_2O experiments as a function of thickness. The blue data points are from the experiments at 10 K, the red points at 100 K. The solid lines represent the fit of $\frac{\delta}{d}$ to the rates. The resulting values of δ are shown in the corresponding color in the figure.

TABLE 5.3: Half-life times of Gly at different locations in the solar system. The final column indicates how thick of a water ice layer would need to be to increase the half-life time to 100 million years.

	VUV flux $cm^{-2}\ s^{-1}$	Half-life time Gly [s]	Thickness d, $t_{\frac{1}{2}}$ = 100 Myr [nm]
Laboratory	$1.7 \cdot 10^{15}$	$3.8 \cdot 10^{2}$	$4.5 \cdot 10^{3}$
Dense Cloud	$1 \cdot 10^{3}$	$6.4 \cdot 10^{14}$	$2.4 \cdot 10^{2}$

decreases as a function of thickness according to Eq. 5.4, the following relation can be established:

$$d_s = -\delta \ln(\frac{I_s}{I_{lab}} \frac{t_s}{t_{\frac{1}{2}}}). \tag{5.7}$$

Using the half-life time of Gly of 380 seconds, the stability of Gly in astronomical environments can now be estimated. In Table 5.3 we show the calculated values for half-life times of Gly in ASW dark cloud conditions. The VUV flux in dark clouds is assumed to be 10^3 photons $cm^{-2}\ s^{-1}$ (Prasad and Tarafdar, 1983; Shen et al., 2004). Using Eq. 5.7, the respective fluxes and the water VUV attenuation factor of $\delta = 152$ nm, we calculate how thick a layer of ice would have to be for embedded Gly to have a half-life time of 100 Myr under these conditions, see Table 5.3.

As the expected thickness of ice on dust grains in dark clouds is at expected to be between a few to a few tens of nm, the required shielding is likely not obtained in these environments purely from H_2O. Possibly though, with the half-life time of Gly being in the order of a few tens of millions of years, part of it may possibly survive and potentially end up in comets, depending on the times it would take before the cloud evolves to collapse and form a star. The lifetime of dark clouds is currently still somewhat of a discussion point within the community. Typical lifetimes for the evolution of a dark cloud into a young stellar object are in the 10-100 Myr range (Bergin and Tafalla, 2007), which is why we use 100 Myr for the calculation in Table 5.3. It should be noted that the numbers in Table 5.3 are upper limits for the required thicknesses, as no other ice constituents are included in the calculation as we only considered the effect of ASW. If one would assume a complex interstellar ice mixture, containing silicate grains, carbonaceous material, PAHs as well as other ice components like methanol and CO_2, the VUV penetration will be less, and as a consequence

less thick ice layers will provide a comparable amount of protection against photodegradation.

5.4 Conclusions

We have shown in a laboratory-based experiment that it is possible to derive the protective properties of ASW in the VUV induced photodegradation process of embedded glycine. We demonstrated the photodestruction of Gly in ASW at different temperatures yield different products. It is found that for pure ASW ices may provide some, but likely not sufficient protection to enable glycine to survive in a dark-cloud for extensive periods of time.

Acknowledgments

Financial support through the NWO PEPSci (Planetary and ExoPlanetary Science) program is acknowledged. VK thanks Jiao He, Arthur Bosman and Trevor Hamlin for helpful discussions. This research has made use of NASA's Astrophysics Data System.